Key Points:
- Submarine permafrost cored in the central Laptev Sea shelf is low in methane
- Degrading submarine permafrost releases methane during thaw
- Methane is oxidized in unfrozen sediment before it reaches the water column

Correspondence to:
P. P. Overduin,
paul.overduin@awi.de

Methane oxidation following submarine permafrost degradation: Measurements from a central Laptev Sea shelf borehole

Pier Paul Overduin[1], Susanne Liebner[2], Christian Knoblauch[3], Frank Günther[1], Sebastian Wetterich[1], Lutz Schirrmeister[1], Hans-Wolfgang Hubberten[1], and Mikhail N. Grigoriev[4]

[1]Alfred Wegener Institute Helmholtz Centre for Polar and Marine Research, Potsdam, Germany, [2]GFZ German Research Centre for Geosciences, Potsdam, Germany, [3]Institute of Soil Science, Center for Earth System Research and Sustainability, Universität Hamburg, Hamburg, Germany, [4]Siberian Branch, Russian Academy of Sciences, Mel'nikov Permafrost Institute, Yakutsk, Russia

Abstract Submarine permafrost degradation has been invoked as a cause for recent observations of methane emissions from the seabed to the water column and atmosphere of the East Siberian shelf. Sediment drilled 52 m down from the sea ice in Buor Khaya Bay, central Laptev Sea revealed unfrozen sediment overlying ice-bonded permafrost. Methane concentrations in the overlying unfrozen sediment were low (mean 20 μM) but higher in the underlying ice-bonded submarine permafrost (mean 380 μM). In contrast, sulfate concentrations were substantially higher in the unfrozen sediment (mean 2.5 mM) than in the underlying submarine permafrost (mean 0.1 mM). Using deduced permafrost degradation rates, we calculate potential mean methane efflux from degrading permafrost of 120 mg m^{-2} yr^{-1} at this site. However, a drop of methane concentrations from 190 μM to 19 μM and a concomitant increase of methane δ^{13}C from −63‰ to −35‰ directly above the ice-bonded permafrost suggest that methane is effectively oxidized within the overlying unfrozen sediment before it reaches the water column. High rates of methane ebullition into the water column observed elsewhere are thus unlikely to have ice-bonded permafrost as their source.

1. Submarine Permafrost on the East Siberian Shelf

Greenhouse gas exchanges between the Earth's atmosphere, the land, and the ocean are being quantified by ongoing research [*McGuire et al.*, 2009]. One poorly quantified stock is associated with submarine permafrost on the arctic continental shelf. Submarine permafrost formation and its subsequent warming and thawing result from the inundation of terrestrial permafrost during the Holocene marine transgression and/or coastal retreat since the Last Glacial Maximum. Permafrost may have three distinct roles mitigating greenhouse gas fluxes in this context: (1) it withholds carbon, by freezing it, from cycling in the global carbon cycle [*Grosse et al.*, 2011]; (2) it acts as a cap on the upward diffusion of biogenic and/or thermogenic gas [*Ruppel*, 2011]; and (3) cold ground can create conditions whereby gas hydrate may be stable at shallower depths than in the marine environment [*O'Connor et al.*, 2010]. Submarine permafrost thaw has thus been invoked as a mechanism for increasing methane efflux from the Siberian shelf seabed to the water column and the atmosphere [*Nicolsky et al.*, 2012; *Shakhova et al.*, 2010]. Underlying assumptions are made that warming of shallow coastal waters has accelerated permafrost thaw and that water columns are short enough to permit methane to reach the ocean-atmosphere interface.

Warming of submarine permafrost increases microbial activity and may destabilize gas hydrates, if present. Thawing of permafrost decreases its ice content and increases sediment permeability which can result in accelerated transport of methane. Methane in the sediment and water column may be thermogenic or biogenic in origin and may have been present in dissolved or gas phases in frozen ground or in gas hydrate form prior to mobilization [*Dallimore and Collett*, 1995]. Based on the position of methane associated with permafrost [*Grosse et al.*, 2011], we differentiate between subpermafrost and intrapermafrost methane. Modeling of permafrost thaw suggests that associated rates of gas hydrate dissociation may increase exponentially [*Frederick and Buffett*, 2014], although the effects of latent heat of dissociation and the position of hydrate deposits relative to the permafrost play an important role [*Taylor et al.*, 2004]. Recent observations of high methane concentrations in the water column and atmosphere in

the Laptev and East Siberian Seas, and observations of methane bubble plumes, are probably associated with pathways for gas flow through the sediment column, which may be created by permafrost thawing [*Shakhova et al.*, 2014]. Major knowledge gaps exist especially in the polar region when it comes to constraining the amount of methane stored in the sediments, its current and potential emission rates into the water column and atmosphere, and the processes that regulate methane production and release from shelf sediments and the ocean [*Ruppel*, 2014]. Due to high sulfate concentrations in seawater, the predominant terminal step of anaerobic oxidation of organic matter in marine sediments is microbial sulfate reduction and not methanogenesis [*Jørgensen*, 1982]. The anaerobic oxidation of methane with sulfate as terminal electron acceptor is globally important in mitigating methane fluxes from the seabed [*Knittel and Boetius*, 2009, and references therein; *Bowles et al.*, 2014]. This process is associated with the sulfate-methane transition zone and in most cases is restricted to shallow (centimeter to meter scale) sediment depths where sulfate has not been depleted by organic matter degradation through sulfate reduction.

Data on the distribution, thickness, and thermal conditions of submarine permafrost across the East Siberian Arctic shelf are sparse. Current maps of submarine permafrost distribution are based on modeling of permafrost development over previous glacial-interglacial cycles [*Nicolsky et al.*, 2012; *Romanovskii and Hubberten*, 2001; *Zhigarev*, 1997]. Modeling suggests that permafrost is distributed continuously across the shallow Laptev shelf; this permafrost did not thaw completely during the last glacial-interglacial transgression, except along active fault and rift zones with high geothermal heat flux or beneath large persistent water bodies [*Nicolsky et al.*, 2012]. Recent results centered on the New Siberian Islands suggest that a more complicated glacial history than used in these models may yield more variable submarine permafrost distribution [*Niessen et al.*, 2013]. In their review of available bottom water temperatures and salinity, *Dmitrenko et al.* [2011a] show recent bottom water warming during the summer months (June–September) close to the coast (<10 m water depth) by less than 2.1°C since around 1985. Such warming may change the thermal regime of submarine permafrost in the Laptev and East Siberian Seas. In the few locations where it has been observed, submarine permafrost temperature is usually around −1°C in coastal waters, close to the limit required to maintain ice-bonded permafrost under submarine conditions [*Grigoriev*, 2008].

We hypothesize that submarine permafrost contains methane and that thawing of this permafrost releases methane from the shelf into the water column. Our objective is to characterize methane concentrations in submarine permafrost and to estimate rates of thaw and methane mobilization from degrading submarine permafrost.

2. Regional Setting

The Laptev, East Siberian, and Chukchi Seas together comprise most of the arctic shelf area and more than 80% of the potential submarine permafrost in the Arctic (Figure 1a). In this region, mean modern coastal erosion rates lie in the range of 1–2 m/yr [*Lantuit et al.*, 2012], result in the creation of about 10 km^2 of submarine permafrost annually [*Grigoriev*, 2008], and may be subject to recent acceleration due to warmer summers and reduced sea ice duration [*Günther et al.*, 2015]. Coastal retreat erodes surface deposits belonging to late Pleistocene Ice Complex and Holocene thermokarst deposits of eastern Siberia [*Schirrmeister et al.*, 2011a, 2011b], transporting this organic-rich unit into the marine realm and exposing the underlying Pleistocene alluvial sands to submarine conditions. Similar sandy deposits of alluvial-fluvial origin, based on stratigraphic position, grain-size distribution, and composition, are found in the western Laptev Sea [*Winterfeld et al.*, 2011], Lena Delta [*Schirrmeister et al.*, 2003, 2011c; *Wetterich et al.*, 2008], and the central Laptev Sea [*Grosse et al.*, 2007; *Kunitsky*, 1989; *Slagoda*, 2004]. Sandy deposits of alluvial origin underlying the Ice Complex are recorded east of Buor Khaya Peninsula from coastal exposures at Vankina Bay [*Katasonov and Pudov*, 1972; *Zhigarev*, 1998], the Dmitry Laptev Strait [*Grigoriev*, 1966; *Konishchev and Kolesnikov*, 1981; *Tumskoy*, 2012], and on the New Siberian Islands [*Andreev et al.*, 2009; *Fartyshev*, 1993] (Figure 1b). These deposits are similarly characterized by their deposition under subaerial conditions (terrestrial permafrost), massive cryostructure (pore ice), lithostratigraphic position (underlying the Ice Complex unit), and silty sand grain size. Organic carbon content of the sediment generally does not exceed 1–2 wt %, which is substantially lower than values characteristic for the overlying deposits composed of Ice Complex (mean total organic carbon (TOC) 3.2 wt %) and Holocene thermokarst (mean TOC 6.2 wt %) deposits [*Strauss et al.*, 2013]. Where the overlying Ice Complex prevents Pleistocene sands
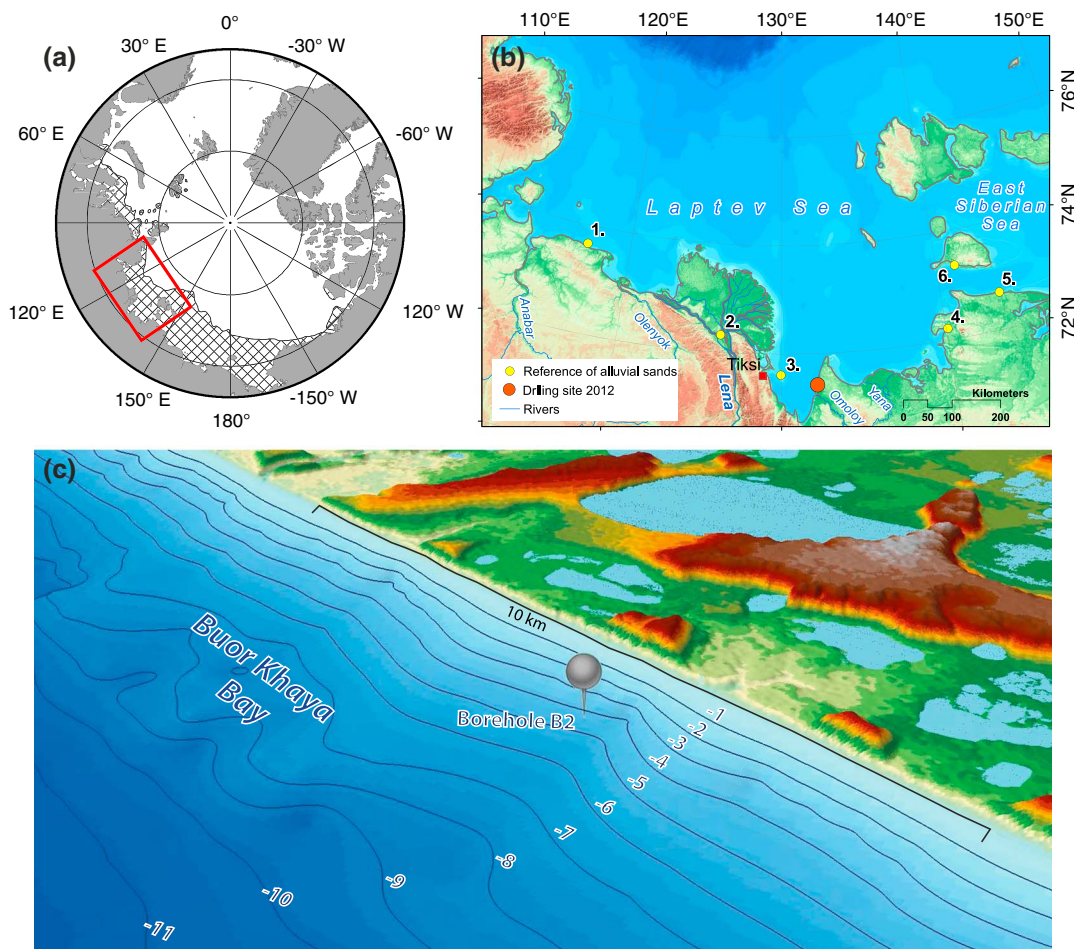
Figure 1. (a) The Laptev Sea (circumpolar perspective map) and potential submarine permafrost extent (striped area, based on *Brown et al.* [2002]) are shown. (b) Described locations of Pleistocene alluvial sands: (1) western Laptev Sea [*Winterfeld et al.*, 2011], (2) Lena Delta [*Schirrmeister et al.*, 2003, 2011a, 2011c; *Wetterich et al.*, 2008], (3) Muostakh Island [*Kunitsky*, 1989; *Slagoda*, 2004], (4) Vankina Bay[*Katasonov and Pudov*, 1972; *Zhigarev*, 1998], (5) Dmitry Laptev Strait [*Grigoriev*, 1966; *Konishchev and Kolesnikov*, 1981; *Tumskoy*, 2012], and (6) New Siberian Islands [*Andreev et al.*, 2009; *Fartyshev*, 1993]. (c) Panoramic view of the drilling site (pin), close to the western shore of the Buor Khaya Peninsula, combining bathymetry with 1 m isobaths from digitized sea charts and topography of a SPOT-5 digital elevation model.

from denudation, their upper extent in the Laptev Sea region lies between 10 m below sea level [*Kunitsky*, 1989], 5 to 12 m above sea level (asl) in the western Laptev Sea [*Schirrmeister et al.*, 2008], and up to about 16 to 21 m asl in the Lena Delta [*Morgenstern et al.*, 2013]. Laptev and East Siberian Sea records of submarine sediment temperature and sediment characteristics are limited to boreholes less than 100 m deep located close to shore (in less than 10 m water depth) [*Grigoriev*, 2008; *Overduin et al.*, 2007; *Winterfeld et al.*, 2011]. *Nicolsky et al.* [2012] model higher geothermal heat flux and modern seabed temperatures (mean observed temperatures from 1999 to 2009), showing the development of an open talik (an area free of ice-bonded permafrost) beneath central Buor Khaya Bay in the central Laptev Sea. These results suggest that Buor Khaya Bay is a region with "warm" submarine permafrost that is undergoing degradation and sensitive to environmental changes.

3. Methods

Sediment drilling was conducted just offshore of the eastern coast of Buor Khaya Bay in the central Laptev Sea (71°25′20.3″N, 132°05′05.3″E; Figure 1c), southeast of the Lena Delta, in April–May 2012 [*Günther et al.*, 2013a]. Following measurements similar to *Overduin et al.* [2012], a geophysical site survey was carried out in 2011 [*Wetterich et al.*, 2011]. Based on this reconnaissance field work, we were assured of encountering

ice-bonded permafrost undergoing degradation at the drill site. Casing was drilled through the sea ice into the seabed, allowing dry drilling using a rotary drill with 4 m casing with diameters between 7 and 12 cm (URB-4T, Vorovskii Factory for Drilling Equipment, Ekaterinburg, Russia). Frozen cores were ejected from the core barrel using compressed air when cold ambient temperatures led to freezing between core and barrel. Unfrozen core sections were immediately frozen at temperatures of less than $-20°C$, so that the outer surface of the core was effectively sealed. All sections were described, packed, catalogued, and transported in a frozen state. The cores were further sectioned, cleaned, photographed, and described with respect to color, organic inclusions, as well as ice and sediment structures after equilibration to $-12°C$ in a climate chamber. The cryostructure of the sediment was described following *French and Shur* [2010].

Borehole temperature was measured using a 40 m Geoprecision thermistor string following a one-point calibration in deionized ice water. Temperature was recorded at 15 min intervals in the borehole for 4 days following drilling, and only temperatures with standard deviations from the mean of less than 0.05°C for the period of record are reported. Temperatures were interpolated linearly to depths at which sediment was sampled to provide values for methane solubility calculations following *Yamamoto et al.* [1976].

Freeze-dried sediment samples were homogenized and split for sedimentological analyses. Hydrogen peroxide was used to remove organic matter, and grain size was analyzed by a Coulter LS 200 laser particle size analyzer. Total organic carbon (TOC) of the bulk sediment was determined using an Elementar Vario EL III. Where sufficient TOC was present, stable carbon isotope ratios (δ^{13}C-TOC) were measured after removal of carbonates with 10% HCl in Ag cups with a Finnigan Delta S mass spectrometer coupled to a FLASH element analyzer and a ConFlo III system. Accuracy of the measurements was determined by parallel analysis of internal and international standard reference material ($CaCO_3$ 12%; NCSDC 73311[GSD-1], China National Center for Iron and Steel, Beijing, China; Marine Sediment, High Purity Standards, Charleston SC, USA; SOIL, LECO Corporation St. Joseph MI, USA; IVA33802150, IVA99994, IVA99995, IVA99996, IVA Analysetechnik, Meerbusch, Germany). The analyses were accurate to ±0.2‰, and values are expressed relative to VPDB (Vienna Peedee belemnite).

The volume and weight of frozen and freeze-dried subsamples were determined for bulk and dry density and total volumetric water content (ice and water). After thawing, pore water was sampled using Rhizons™ with an effective pore size of 0.1 μm. Pore water salinity was measured using a WTW MultiLab 540 electrical conductivity meter with a TetraCon™ 325 cell referenced to 20°C. Salinities are reported without units, based on the practical salinity scale. Sulfate concentrations (in millimolar, mM) were determined using a KOH eluent and a latex particle separation column on a Dionex DX-320 ion chromatographer. The dissolved organic carbon (DOC) concentration in the sediment pore water was measured as nonpurgeable organic carbon via catalytic combustion at 680°C using a Shimadzu TOC-VCPH instrument on samples treated with 20 μL of 30% suprapure hydrochloric acid. Stable water isotopes (δD and δ^{18}O) were analyzed following *Meyer et al.* [2000] on equilibrated samples using a Finnigan MAT Delta S mass spectrometer. Values are reported as per mille difference from the Vienna standard mean ocean water. Standard deviations were better than 0.5‰ for δD and 0.1‰ for δ^{18}O.

Frozen subsamples were taken from the core using ice screws at 80 depths between 2 and 47.5 m below seafloor (bsf). They were immediately immersed in a saturated NaCl solution to drive gases out of solution and capped with a septum for later determination of methane and carbon dioxide concentrations and the stable carbon isotope composition of the methane (δ^{13}C-CH$_4$). Methane and carbon dioxide concentrations in the headspace were measured with an Agilent GC 7890 equipped with a Ni catalyst to reduce carbon dioxide to methane, a flame ionization detector and a Porapak-Q column. Helium served as carrier gas. The amount of gas in the vials was calculated from headspace concentrations, gas pressure and solubility, and the volume of liquid in the bottles. Methane and carbon dioxide concentrations are reported relative to sediment pore water volume, regardless of whether present as ice or water, based on calculated total sediment water content.

The δ^{13}C-CH$_4$ values were determined with a Finnigan Delta Plus isotopic ratio mass spectrometer equipped with a PreCon and a GC/C III interface [*Brand*, 1995]. The precision of the measurement was generally better than ±0.5‰. Measured values were corrected with internal ($-43.8‰$) and external (National Institute of Standards, USA, RM8561; $-73.27‰$) methane standards that were both measured after a maximum of 10 analyses. All stable carbon isotope values are expressed relative to VPDB.
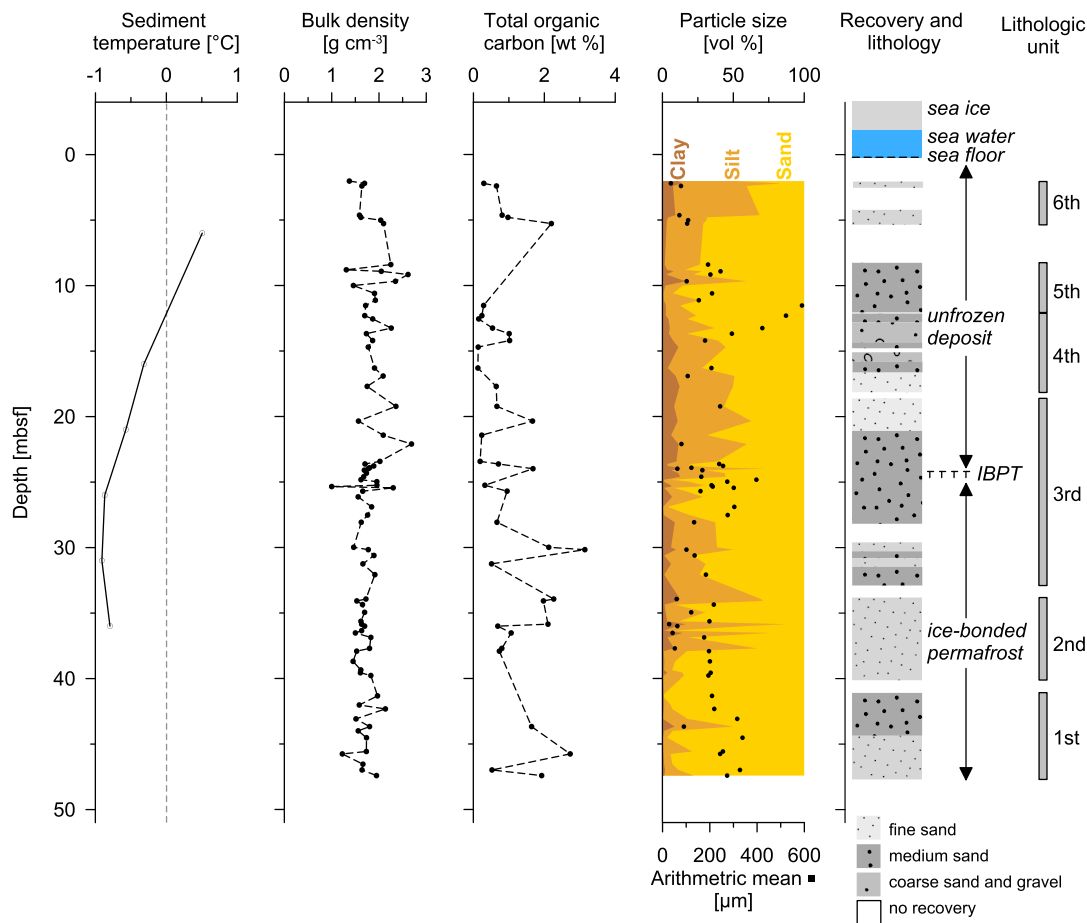
Figure 2. Sediment characteristics, from left to right: in situ temperature, wet bulk density, total organic carbon (TOC) content, particle size distribution (upper axis) and means (lower axis), and cryolithology. Sea ice thickness and seawater depth are shown at the top of the right-hand graph; the depth of the ice-bonded permafrost table (IBPT) is indicated on the right.

Data sets for statistical analysis were tested for normal distribution using the Shapiro-Wilk test. Due to nonnormal data distribution, a Man-Whitney rank sum test was performed to compare selected data sets and Spearman's rank correlation coefficients for correlation analysis using IBM SPSS 18.

4. Results

Drilling from a 2 m thick sea ice cover, 35 m of core were recovered between 2 and 48 m bsf with a recovery rate of 78.4%. The borehole was located approximately 750 m from the modern coastline in 4 m deep water. Ice-bonded sediment was encountered at 24.75 m bsf, with 24.7 m of overlying unfrozen sediment. The sharp boundary between unfrozen and frozen sediments was recovered within one core section. Borehole temperatures ranged between −1.0 and −0.5°C and between 6 and 36 m bsf, with temperatures higher than −0.8°C in the overlying unfrozen sediment and between −1.0 and −0.8°C in the frozen sediment (Figure 2).

The sediment had a mean dry bulk density of 1.7 ± 0.7 g cm^{-3} and total organic carbon (TOC) contents less than 3.1 wt % (mean: 0.5 ± 0.8 wt %, $n = 37$), with most values below the detection limit of 0.1 wt % (Figure 2). Isolated, numerous layers up to several centimeters thick consisting of woody detritus up to 3 cm in diameter were found throughout the core, in which organic content probably locally exceeded measured values. Below 24.75 m bsf, ice was almost entirely present as pore ice in massive cryostructures, with occasional isolated microlens-like cryostructures (thin ice veins less than 1 mm thick).
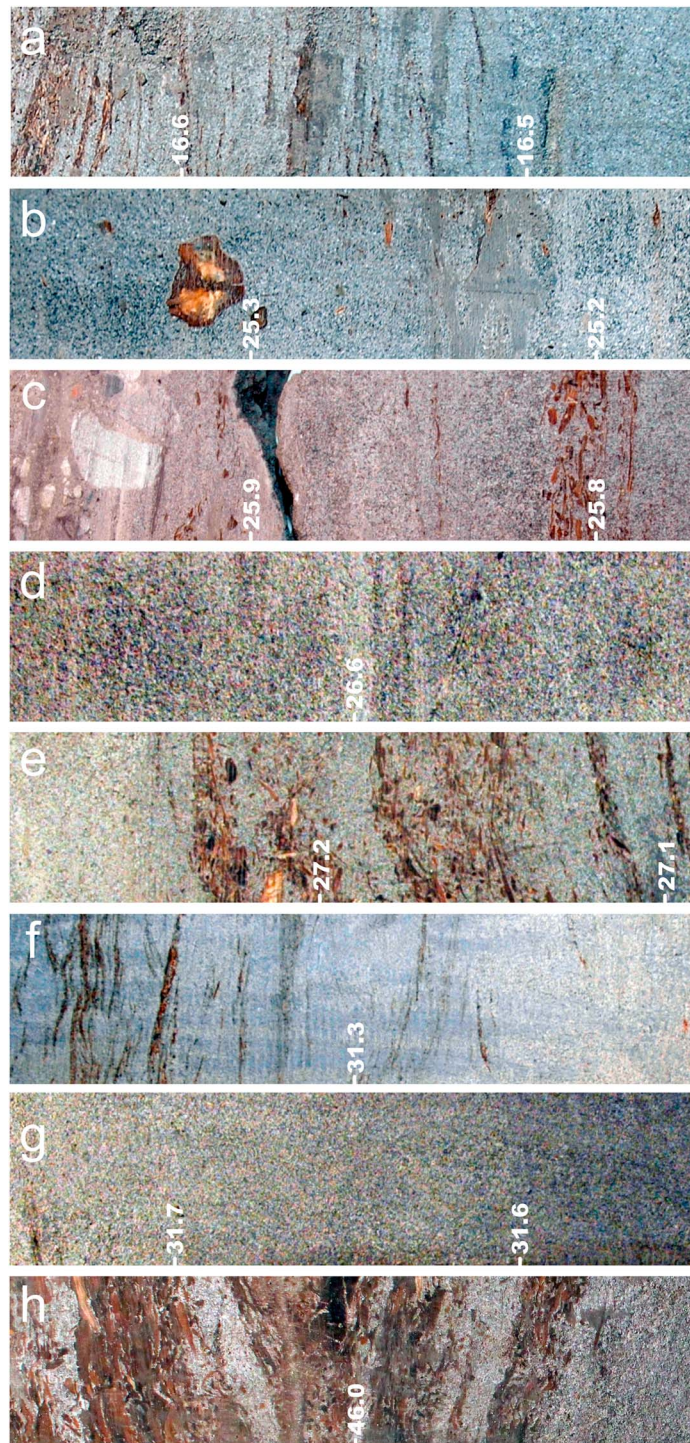
Figure 3. Photos of selected core sections, 20 cm wide and 5 cm high, oriented with the downcore direction to the left. (a) Unfrozen, midgrained sand, weakly bedded, single coarse wood remains, and organic layers <2 mm thick (fourth unit). The following images show ice-bonded sediment: (b) midgrained sand, microlens-like cryostructure, and organic remains, including approximately 2 cm diameter woody stem at 25.3 m (third unit); (c) microlens-like cryostructure, wooden detritus at 29.8 m and below 25.9 m, and midgrained sand with gravel inclusions around 25.95 m; black section is a break in the core (third unit); (d) microlens-like to massive cryostructure and midgrained sand (third unit); (e) microlens-like cryostructure, wooden detritus from 26.09 to 27.25 m inclined at up to 16°, and midgrained sand (third unit); (f) fine-grained sand, bedded plant detritus layers up to 1 mm thick, and with a massive cryostructure (third unit); (g) midgrained sand, without bedding, no organic material visible, and massive cryostructure; and (h) bedded, fine-grained sand, massive cryostructure, plant detritus, and wood remains bedded in layers inclined at up to 20° (first unit).
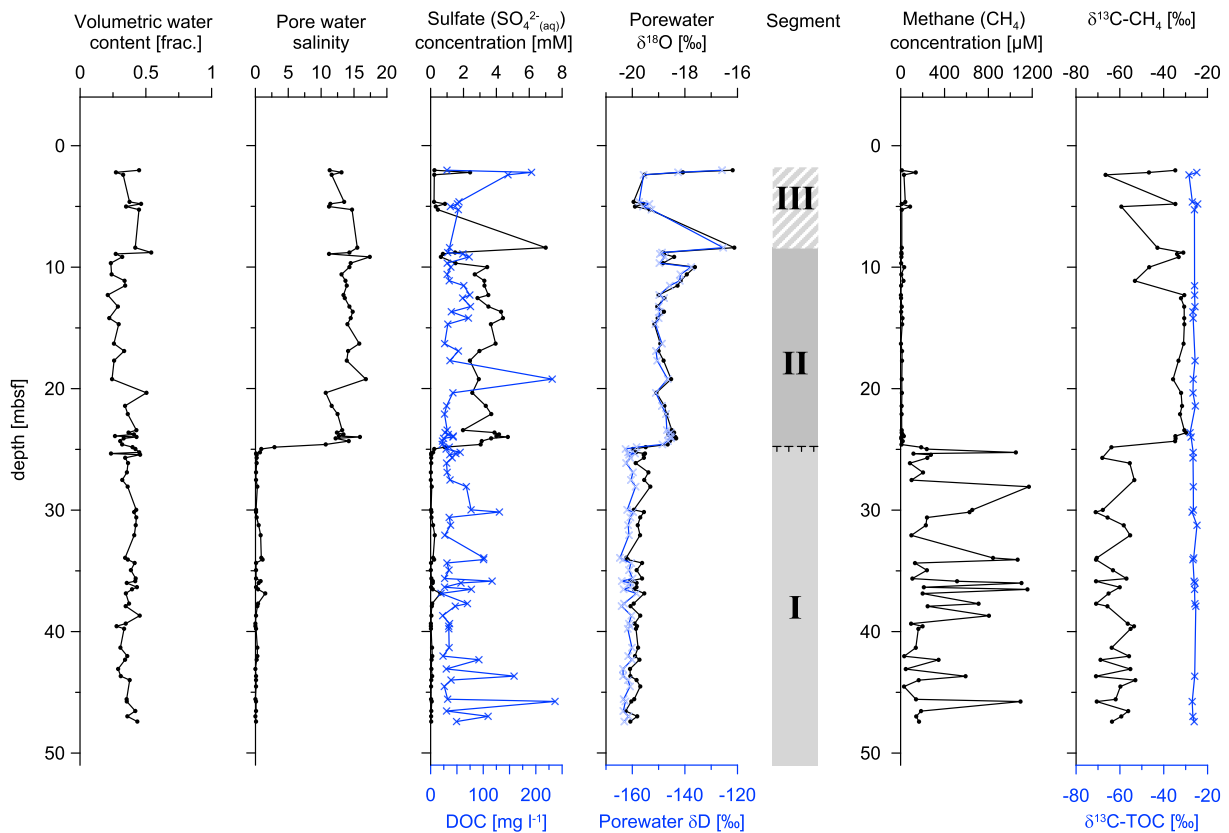
Figure 4. Pore water characteristics, from left to right: volumetric water content, pore water salinity, sulfate, and dissolved organic carbon concentrations ($[SO_{4(aq)}^{2-}]$: upper axis and DOC: lower axis, respectively) and water stable isotope ratios ($\delta^{18}O$: upper axis and δD: lower axis) as a function of depth below seafloor (mbsf). The classification into permafrost segments (I, II, and III) is based on sediment cryolithology, pore water chemistry, and inferred permafrost dynamics. The two graphs on the right-hand side show methane concentrations ($[CH_4]$) and $\delta^{13}C$ ratios in the methane ($\delta^{13}C$-CH_4: upper axis) and sediment total organic carbon ($\delta^{13}C$-TOC: lower axis).

The lowermost first unit (41.10–47.55 m bsf; Figure 2) consisted of alternations of partly bedded grey (silty), medium- and coarse-grained sands with organic spots, plant detritus, and occasional layers of wood remains (Figure 3). The cryostructure was massive. The second unit (33.85–40.10 m bsf) was characterized by partly bedded grey (brown) sandy silt and medium- and coarse-grained sands with organic spots and plant remains and microlens-like and massive cryostructures. The third unit (18.60–32.80 m bsf) was composed of cross- and horizontal-bedded grey silty fine-grained sand layers and of nonbedded medium- and coarse-grained sands with plant and wood remains. The cryostructure was dominantly microlens-like. The boundary between the unfrozen and ice-bonded segments marked by the ice-bonded permafrost table (IBPT) at 24.75 m bsf did not exhibit changes in sediment characteristics and is therefore not assumed to have been a geological boundary. The IBPT was clearly defined by changes in (a) the presence/absence of ice, (b) pore water salinity and related changes in pore water chemical and isotopic composition, and (c) methane concentrations and $\delta^{13}C$-CH_4 signatures (described below in Figures 2 and 4). The unfrozen fourth unit (12.15–18.1 m bsf) was an alternation of horizontal-bedded grey silt, bedded and nonbedded medium- and coarse-grained sands with single dark organic plant detritus and single wood fragments. Further up, the fifth unit (8.25–12.00 m bsf) was composed of layers of nonbedded fine-, medium-, and coarse-grained sands with some pebbles (up to 2 cm in diameter) and coarse wood fragments. The uppermost sixth unit (2.00–5.35 m bsf) was composed of partly bedded grey silty fine-grained sand that contains thin dark layers of plant detritus and wood fragments.

Mean volumetric total water contents in the sediment were 0.4 ± 0.1 (Figure 4). Mean pore water salinity was 13.5 ± 1.6 in the unfrozen and 0.4 (range: 0–0.9) in the ice-bonded sediment and varied between
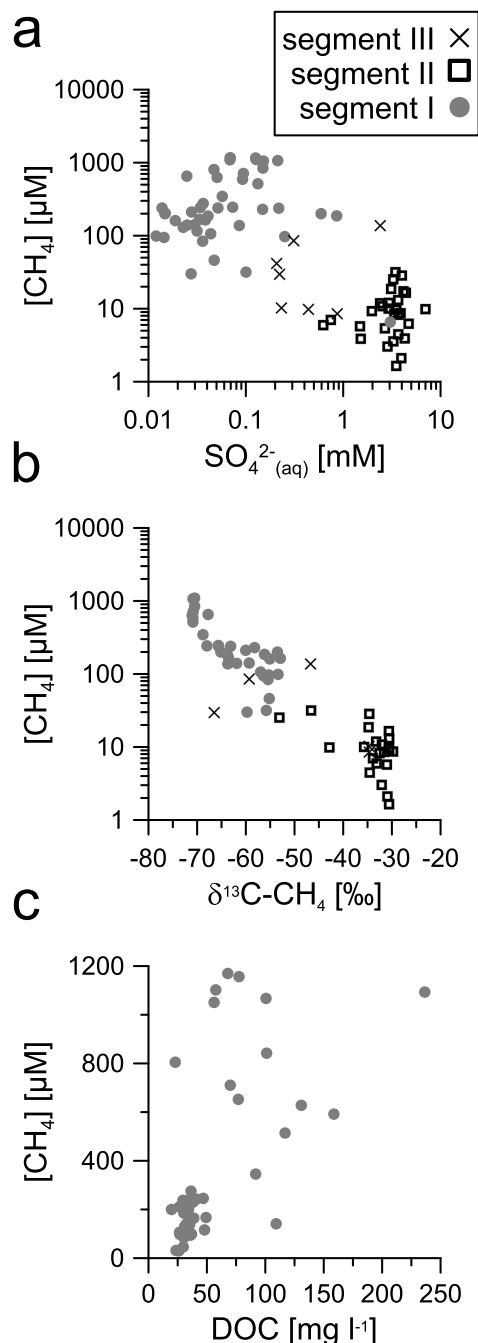
Figure 5. Scatterplots of methane concentration and (a) sulfate concentration, (b) $\delta^{13}C$ ratio of methane, and (c) dissolved organic carbon (DOC). The upper graphs show data for the entire core; the lower graph shows only the frozen portion of the core.

<0.1 and 17.4, from fresh to brackish water. Sulfate concentration profiles in the unfrozen layers suggested varying degrees of marine influence with a mean sulfate concentration of 2.5 ± 1.5 mM (Figure 4). At the thaw front, sulfate concentration values decreased by 2 orders of magnitude over a depth range of about 60 cm. In the frozen layers, mean sulfate concentrations were 0.1 mM (range: 0–0.25 mM) in the bulk pore water after thawing. In the frozen sediment, most of this sulfate probably exists in water remaining unfrozen at the interfaces between pore ice and sediment grains. Local concentrations of sulfate could therefore be higher, depending on the degree to which pore water is present as ice. Dissolved organic carbon (DOC) concentrations ranged from 20 to 240 mg L^{-1}, with a mean of 53 ± 39 mg L^{-1}. Pore water stable isotope signatures also changed at the IBPT, from δD greater than -158‰ in the overlying unfrozen sediment ($\delta^{18}O$: -20.0 to -16.1‰) to less than -158‰ in the ice-bonded sediment ($\delta^{18}O$: -20.3 to -19.3‰) (Figure 4). The $\delta^{13}C$-TOC values for the sediment organic matter ranged between -28.5‰ and -24.5‰ (mean -26.3 ± 0.8‰, for 33 samples with TOC > 0.2 wt %; Figure 4).

Methane concentrations and stable carbon isotope signatures of methane significantly differed between the overlying unfrozen sediment layers above 24.75 m bsf and the ice-bonded layers below ($p < 0.01$; Figure 4). Methane concentrations in the overlying unfrozen sediment were generally lower (1.6 to 137.2 µM; mean: 17.1 ± 24.9 µM) than in the frozen layers (30 to 1169 µM; mean: 380.6 ± 354.9 µM). Carbon dioxide concentrations were not significantly different in the overlying unfrozen sediment (0.2 to 49.4 mM; mean: 10.1 mM, $n = 22$) and in the frozen sediment (1.2 to 17.7 mM; mean: 5.0 mM, $n = 19$). Stable carbon isotope values of methane were higher in the overlying unfrozen sediment (-66.5‰ to -29.8‰; mean: -36.9 ± 9.3‰) than below 24.75 m bsf (-71.0‰ to -53.0‰; mean: -62.4 ± 6.5‰). Methane concentrations were negatively correlated to sulfate concentrations (Spearman's $\rho = -0.676$, $p < 0.001$, $n = 80$; Figure 5a) and methane carbon isotope signatures ($\rho = -0.897$,

$p < 0.001$, $n = 60$; Figure 5b). A significant correlation between methane concentrations and DOC concentrations was found only in the frozen layers ($\rho = 0.625$, $p < 0.001$, $n = 43$; Figure 5c) but not in unfrozen ones ($\rho = 0.172$, $p = 0.310$, $n = 37$). Methane concentrations were less than 10% of saturation at the observed total pore water content and its salinity, temperature, and pressure (based on hydrostatic pressure) throughout the core.

5. Discussion

5.1. Permafrost Dynamics

Inundation of terrestrial permafrost usually leads to its eventual degradation, especially when the overlying water reaches depths exceeding the annual sea ice thickness and when the mean annual sea bottom water temperatures between the freezing point of seawater and peak summer temperatures warm the permafrost from above [*Osterkamp*, 2001]. Not only increased heat transfer to the sediment results in degradation of permafrost: advective and diffusive penetration of salt from saline bottom water (8.9 to 31.5‰ in the Buor Khaya Bay, according to *Charkin et al.* [2011]) lowers the freezing temperature of the interstitial pore water of the permafrost. Both processes lead to permafrost thaw, i.e., degradation. The recovered submarine sediment can be classified into three segments (Figure 4): (I) a lower, frozen portion of terrestrial origin (24.75 to 48 m bsf), overlain by (II) terrestrial deposits that have thawed under marine influence, overlain by (III) marine sediments reworked by wave and sea ice action near the seabed. The boundaries between segments are not clearly reflected in the sediment stratigraphy. The boundary between segments II and III probably lies around 6 m bsf, above which higher variability in sediment TOC and in pore water stable isotope ratios and salinity suggest changes in sediment source and the composition of overlying seawater. *Heim et al.* [2014] describe increased turbidity following storms in the study region (Buor Khaya Bay, Laptev Sea) at locations with water less than around 10 m deep, supporting this observation.

At the site drilled in this study, the sediment cryostratigraphy and fresh pore water with light stable water isotope ratios in the lower ice-bonded segment I of the core indicate deposition under cold, terrestrial conditions that led to freezing of the ground from the surface. According to the granulometric results and sediment structures, partly bedded silty fine- to coarse-grained sands with plant detritus and wood fragment layers were most likely formed in an alluvial environment under changing accumulation conditions (e.g., meandering or braided river floodplains). Pore water is comparatively saline (10–17) from the seabed down to the position of the freeze/thaw transition, which suggests that the transport of seawater through the overlying unfrozen sediment to the thaw front is dominantly convective rather than diffusive [*Harrison and Osterkamp*, 1982; *Chuvilin et al.*, 2013] and that seawater is not limited at the freezing front. Such convection may be driven by density and temperature differences between seawater at the sediment-water interface and freshwater from the thaw front [*Hutter and Straughan*, 1999]. The greater sulfate concentration variability in segment III than in segment II is not reflected in the overall salinity of pore water but follows the stable isotope ratios closely, with the exception of the sample closest to the seafloor (at 2 m bsf). This suggests that seafloor dynamics rather than postdepositional microbial activity in the sediment have led to the observed variations. Benthic water in this region changes from brackish seawater to relatively fresh fluvial water depending on pycnocline depth [*Dmitrenko et al.*, 2011b], which varies on seasonal and shorter time scales. In addition, sediment deposition on the seafloor, its resuspension by waves during storm events in the fall, and disturbance by ice in the spring can all affect profiles of sediment composition and pore water chemistry in segment III. Core recovery in segment III was less than 50% (Figure 1), so that more detailed analysis of the relative roles of depositional and postdepositional changes to pore water chemistry is difficult.

Currently, onshore ground temperatures on the Buor Khaya Peninsula are about −10°C at 20 m depth [*Günther et al.*, 2013a], and permafrost extends down to around 600 m below the ground surface [*Romanovskii et al.*, 2004]. The upper, unfrozen segment (II) of the core probably thawed following flooding. As a result, sediment throughout the core has warmed from −10°C to temperatures near the freezing point. The Buor Khaya Peninsula is about 85% covered by thermokarst depressions [*Günther et al.*, 2013b], and we cannot exclude the possibility that the borehole site was affected by Holocene thermokarst or thermokarst lake development prior to erosion. The drill site is located offshore of an eroding Ice Complex coastal bluff (Figure 1c), making it likely that the drill site was frozen at the time that it was flooded.

The mean rate of permafrost degradation since inundation can be estimated by comparing the distance of the borehole from the coast to the modern coastline retreat rate and assuming that (a) mean annual erosion rates have not changed during this period and (b) that the profile was frozen prior to inundation. The approximately 70 km long western coastline of the Buor Khaya Peninsula has been eroding along most of its length at a mean annual rate of 0.5 m yr^{-1} for the past 42 years and at 1.4 ± 0.8 m yr^{-1} along a segment closest to the borehole site [*Günther et al.*, 2012], where the coastline exposes an Ice Complex upland (described below). This is more rapid than the local mean long-term rate of coastal retreat for the

Buor Khaya coast but lower than the mean of $2.2 \, \text{yr}^{-1}$ for the erosional coasts of the Laptev Sea [*Günther et al.*, 2013b]. Based on these values and assuming that coastal erosion rates have varied negligibly since the high stand of the Holocene transgression was reached 5 cal ka [*Bauch et al.*, 2001], the borehole site was flooded around 540 years ago, which would mean that the ice-bonded permafrost has degraded to its current position at 24.75 m bsf at a mean rate of $5.3 \pm 2.7 \, \text{cm} \, \text{yr}^{-1}$. This value falls within the range of observed submarine permafrost degradation rates near the coast (<10 m water depth), which lie between 1 and $15 \, \text{cm} \, \text{yr}^{-1}$ at 12 sites with varying geomorphology and coastline change rates in the Laptev and East Siberian Seas [*Overduin et al.*, 2007].

5.2. Methane in Degrading Permafrost

We present data on methane concentrations and stable carbon isotope signatures in thawing submarine permafrost of the East Siberian shelf. To estimate rates of methane release from degrading permafrost, methane concentrations were integrated over the frozen sections of the core, implicitly assuming that methane concentrations were representative for the core sections from which they were sampled. This is equivalent to a core-section length-weighted mean methane concentration for the frozen portion of the core and gives the amount of methane observed over this length. The resulting methane concentration per volume of ice-bonded permafrost for segment I is $2.3 \pm 2.1 \, \mu\text{g} \, \text{CH}_4 \, \text{cm}^3$ (for which the standard deviation of the concentration is taken as the uncertainty). Combined with the estimate for permafrost degradation rate, this suggests that thawing of the recovered frozen core releases interstitial methane at a mean rate of $2.1 \pm 1.2 \, \text{nmol} \, \text{cm}^{-3} \, \text{d}^{-1}$ or $121 \pm 64 \, \text{mg} \, \text{m}^{-2} \, \text{yr}^{-1}$. Measured methane concentrations in the frozen sediment layers are similar to the values in frozen sub-Ice Complex alluvial sands 12 km offshore in the western Laptev Sea (mean: $365 \, \mu M$, $n = 43$; recalculated from *Koch et al.* [2009] and *Winterfeld et al.* [2011]), where mean submarine permafrost degradation rates are lower ($1–2 \, \text{cm} \, \text{yr}^{-1}$). Methane concentrations in Holocene surface deposits or late Pleistocene Ice Complex permafrost deposits that overlie these alluvial sands are typically higher (mean: $1400 \, \mu M$, $n = 67$; recalculated from *Bischoff et al.* [2013]).

Throughout segment II and at the boundary between unfrozen and frozen sediments, sulfate is present at up to at least $4 \, \text{m}M$. Solute exclusion from ice in the pore space may result in higher concentrations locally in the unfrozen pore water. The deep penetration of sulfate into the sediment indicates slow sulfate consumption by sulfate-reducing bacteria due to limited anaerobic organic matter degradation. The low temperature, low organic matter content, and presumably also low reactivity of the carbon under anaerobic conditions [*Knoblauch et al.*, 2013] restrain microbial activity in the overlying unfrozen sediments. There is no indication for methanogenesis in the thawed permafrost layers of segment II. In the presence of elevated sulfate concentrations, sulfate-reducing microorganisms out-compete methanogenic archaea [*Lovley et al.*, 1982]. Therefore, sulfate reduction is the most important pathway of anaerobic organic matter degradation in marine sediments [*Jørgensen*, 1982]. The stable isotope signatures of methane in the frozen part of the sediment are typical for those found in anaerobic layers of water-saturated soils with active microbial methanogenesis including those affected by permafrost [*Dorodnikov et al.*, 2013; *Hodgkins et al.*, 2014; *Popp et al.*, 1999; *Preuss et al.*, 2013]. The sharp decrease of methane concentrations and increase of $\delta^{13}\text{C-CH}_4$ values at the interface between frozen and overlying unfrozen sediment layers strongly indicate microbial methane oxidation with sulfate as terminal electron acceptor [*Fossing et al.*, 2000; *Meister et al.*, 2013; *Whiticar*, 1999] at or immediately above the interface between segments I and II. A similarly steep gradient of methane concentrations and stable carbon isotope values of methane can also be found in water-saturated soils across the boundary between aerobic and anaerobic conditions where molecular oxygen instead of sulfate serves as electron acceptor for methane oxidation [*Preuss et al.*, 2013; *Whalen and Reeburgh*, 2000]. The observed high sulfate concentration throughout the overlying unfrozen layer delivers large amounts of sulfate to the thaw front. The decrease in sulfate at the thaw front is primarily the result of the impermeability of lower ice-bonded sediment and not controlled by methane release rates. The oxidation of methane after thawing results in methane concentration less than $20 \, \mu M$ in the unfrozen layer above the ice-bonded permafrost, preventing methane from the thawed permafrost from reaching the overlying bottom water, as long as methane transport is diffusive.

We cannot exclude the possibility that dissolved and vapor-phase gas concentrations in the ice-bonded and overlying unfrozen sediment (segments I and II) were affected differently by coring. Pressure changes associated with core recovery may have resulted in higher rates of degassing from the
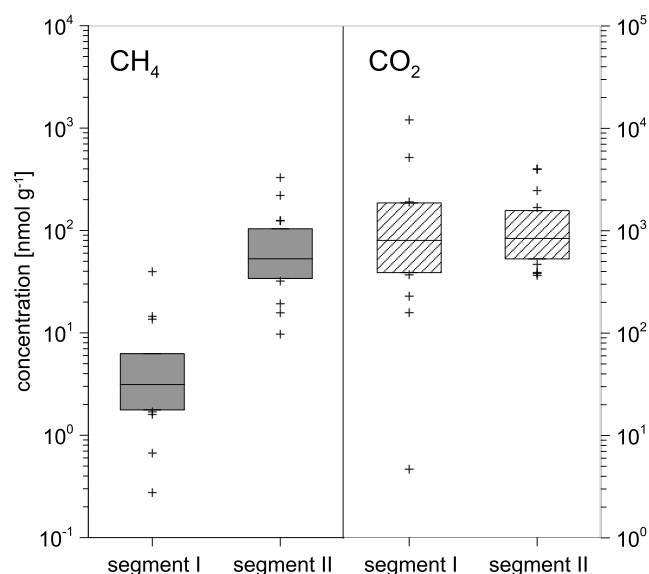
Figure 6. The distribution of (left) measured methane and (right) carbon dioxide concentrations in segments I (ice-bonded) and II (unfrozen) expressed in nmol/g dry sediment, determined in each case on the same samples.

unfrozen sediment, leading to lowering of methane concentrations, for example. This source of uncertainty is difficult to constrain without pressure coring or in situ methods for dissolved methane concentration determination in the sediment column. Two factors suggest that the lower methane concentrations measured in segment II are not the result of degassing, however. Carbon dioxide measurements made on the same samples showed no statistically significant difference between segments I and II, whereas methane did (Figure 6). Second, the stable carbon isotope signatures of methane in the two segments also differed significantly, a fractionation effect consistent with microbial methane oxidation, but not with sampling effects.

Submarine permafrost degradation plays a unique role in marine carbon dynamics. Inundation and subsequent thawing of frozen sediment containing organic matter deliver organic carbon and methane stored in permafrost to the sediment column. In contrast to marine sediments, where organic carbon is deposited on the seafloor [*Judd*, 2004], permafrost thaw releases carbon to the unfrozen sediment column at the IBPT, whose position changes over time. Penetration of sulfate, serving as electron acceptor for anaerobic organic matter and methane oxidation, creates a capacity of the overlying unfrozen sediment column to oxidize released methane. Therefore, it is unlikely that thawing submarine permafrost is a substantial methane source for the overlying water column. Permafrost degradation may be associated with creating pathways for methane release from other sources, such as gas deposits within or below permafrost [*Dallimore and Collett*, 1995; *Yakushev and Chuvilin*, 2000]. Since the unfrozen sediment above the IBPT contains low amounts of methane and elevated sulfate concentrations, which favor sulfate reduction instead of methane production, it is unlikely that degrading submarine permafrost is the source of methane ebullition to the water column of the central Laptev Sea shelf.

6. Conclusions

The texture, low organic carbon content (mean: 0.5 wt %, range: 0.1–3.2 wt %) and moderate mean degradation rate ($5.3 \pm 2.7 \, \mathrm{cm \, yr^{-1}}$) of submarine permafrost drilled in the central Laptev Sea are similar to other regions of the East Siberian Arctic shelf. Methane concentrations in the ice-bonded permafrost are higher than those in the overlying unfrozen sediment. As a consequence of thaw, methane present in submarine permafrost is released within the sediment column at approximately 25 m below the seafloor at a rate of $2.1 \pm 1.2 \, \mathrm{nmol \, cm^{-3} \, d^{-1}}$ (or $121 \pm 64 \, \mathrm{mg \, m^{-2} \, yr^{-1}}$). The observed profiles of sediment pore water sulfate concentrations, as well as methane concentrations and stable carbon isotope ratios, indicate that methane from ice-bonded permafrost is oxidized at or immediately following thaw. Anaerobic oxidation of methane in the unfrozen sediment column between ice-bonded permafrost and the seabed makes it unlikely that methane from thawing submarine permafrost could reach the seabed. Based on these results, recent observations of methane release from the seabed in the study region do not derive from the degradation of submarine permafrost but are probably associated with methane from other sources that can permeate through permafrost-free sediment. One core is not sufficient to capture all processes related to permafrost thawing on the Siberian shelf; further studies should include the analyses of methane from more borehole sites in a variety of sites differing in geomorphology, period of inundation, and permafrost thaw rates.

References

Andreev, A. A., et al. (2009), Weichselian and Holocene palaeoenvironmental history of the Bol'shoy Lyakhovsky Island, New Siberian Archipelago, Arctic Siberia, *Boreas*, *38*, 72–110, doi:10.1111/j.1502-3885.2008.00039.x.

Bauch, H. A., T. Mueller-Lupp, E. Taldenkova, R. F. Spielhagen, H. Kassens, P. M. Grootes, J. Thiede, J. Heinemeier, and V. V. Petryashov (2001), Chronology of the Holocene transgression at the north Siberian margin, *Global Planet. Change*, *31*, 125–139, doi:10.1016/S0921-8181(01)00116-3.

Bischoff, J., K. Mangelsdorf, A. Gattinge, M. Schloter, A. N. Kurchatova, U. Herzschuh, and D. Wagner (2013), Response of methanogenic archaea to late Pleistocene and Holocene climate changes in the Siberian Arctic, *Global Biogeochem. Cycles*, *27*, 305–317, doi:10.1029/2011GB004238.

Bowles, M. W., J. M. Mogollón, S. Kasten, M. Zabel, and K.-U. Hinrichs (2014), Global rates of marine sulfate reduction and implications for sub-sea-floor metabolic activities, *Science*, doi:10.1126/science.1249213.

Brand, W. A. (1995), Precon: A fully automated interface for the pre-GC concentration of trace gases in air for isotopic analysis, *Isot. Environ. Health Stud.*, *31*, 277–284.

Brown, J., O. J. Ferrians Jr., J. A. Heginbottom, and E. S. Melnikov (2002), *Circum-Arctic Map of Permafrost and Ground-Ice Conditions, Version 2*, Natl. Snow and Ice Data Cent., Boulder, Colo.

Charkin, A. N., O. V. Dudarev, I. P. Semiletov, A. V. Kruhmalev, J. E. Vonk, L. Sánchez-García, E. Karlsson, and Ö. Gustafsson (2011), Seasonal and interannual variability of sedimentation and organic matter distribution in the Buor-Khaya Gulf: The primary recipient of input from Lena River and coastal erosion in the southeast Laptev Sea, *Biogeosciences*, *8*, 2581–2594, doi:10.5194/bg-8-2581-2011.

Chuvilin, E. M., B. A. Bukhanov, V. E. Tumskoy, N. E. Shakhova, O. V. Dudarev, and I. P. Semiletov (2013), Thermal conductivity of bottom sediments in the region of Buor-Khaya Bay (shelf of the Laptev Sea) [in Russian], *Earth Cryosphere*, *17*(2), 32–40.

Dallimore, S. R., and T. S. Collett (1995), Intrapermafrost gas hydrates from a deep core hole in the Mackenzie Delta, Northwest Territories, Canada, *Geology*, *23*, 527–530, doi:10.1130/0091-7613.

Dmitrenko, I. A., S. A. Kirillov, L. B. Tremblay, H. Kassens, O. A. Anisimov, S. A. Lavrov, S. O. Razumov, and M. N. Grigoriev (2011a), Recent changes in shelf hydrography in the Siberian Arctic: Potential for subsea permafrost instability, *J. Geophys. Res.*, *116*, C10027, doi:10.1029/2011JC007218.

Dmitrenko, I. A., V. V. Ivanov, S. A. Kirillov, E. L. Vinogradova, S. Torres-Valdes, and D. Bauch (2011b), Properties of the Atlantic derived halocline waters over the Laptev Sea continental margin: Evidence from 2002 to 2009, *J. Geophys. Res.*, *116*, C10024, doi:10.1029/2011JC007269.

Dorodnikov, M., M. Marushchak, C. Biasi, and M. Wilmking (2013), Effect of microtopography on isotopic composition of methane in porewater and efflux at a boreal peatland, *Boreal Environ. Res.*, *18*(3–4), 269–279.

Fartyshev, A. I. (1993), *Osobenosti pribrezhno-shel'fovoi kriolitozony morya Laptevykh (Characteristics of the Coastal-Shelf Permafrost Zone of the Laptev Sea)* [in Russian], 136 pp., Nauka, Novosibirsk, Russia.

Fossing, H., T. G. Ferdelman, and P. Berg (2000), Sulfate reduction and methane oxidation in continental margin sediments influenced by irrigation (southeast Atlantic off Namibia), *Geochim. Cosmochim. Acta*, *64*(5), 897–910, doi:10.1016/S0016-7037-899-900349.

Frederick, J. M., and B. A. Buffett (2014), Taliks in relict submarine permafrost and methane hydrate deposits: Pathways for gas escape under present and future conditions, *J. Geophys. Res. Earth Surface*, *119*, 106–122, doi:10.1002/jgrf.20192.

French, H., and Y. Shur (2010), The principles of cryostratigraphy, *Earth Sci. Rev.*, *101*(3–4), 190–206, doi:10.1016/j.earscirev.2010.04.002.

Grigoriev, M. N. (2008), Kriomorphogenez i litodinamika pribrezhno-shelfovoi zony morei Vostochnoi Sibiri (Cryomorphogenesis and lithodynamics of the East Siberian near-shore shelf zone), Habilitation thesis, Melnikov Permafrost Institute, Russian Academy of Sciences, Siberian Branch [in Russian], Yakutsk, 315 pp.

Grigoriev, N. F. (1966), *Mnogoletnemerzlye porody primorkoi zony Yakutii (Permafrost of the Yakutian Coastal Zone)* [in Russian], 180 pp., Nauka, Moscow.

Grosse, G., L. Schirrmeister, C. Siegert, V. V. Kunitsky, E. A. Slagoda, A. A. Andreev, and A. Y. Dereviagin (2007), Geological and geomorphological evolution of a sedimentary periglacial landscape in northeast Siberia during the late Quaternary, *Geomorphology*, *86*(1–2), 25–51, doi:10.1016/j.geomorph.2006.08.005.

Grosse, G., V. Romanovsky, T. Jorgenson, K. W. Anthony, J. Brown, and P. P. Overduin (2011), Vulnerability and feedbacks of permafrost to climate change, *Eos Trans. AGU*, *92*(9), doi:10.1029/2011EO090001.

Günther, F., P. P. Overduin, A. V. Sandakov, G. Grosse, and M. N. Grigoriev (2012), Thermo-erosion along the Yedoma Coast of the Buor Khaya Peninsula, Laptev Sea, East Siberia, in *Proceedings of the Tenth International Conference on Permafrost, Salekhard, Yamal-Nenets Autonomous District, Russia, June 25–29*, vol. 1, edited by K. M. Hinkel, pp. 137–142, The Northern Publisher, Salekhard, Russia.

Günther, F., P. P. Overduin, A. S. Makarov, and M. N. Grigoriev (Eds.) (2013a), Russian-German Cooperation SYSTEM LAPTEV SEA: The Expeditions Laptev Sea—Mamontov Klyk 2011 & Buor Khaya 2012, Berichte zur Polar- und Meeresforschung, 664.

Günther, F., P. P. Overduin, A. V. Sandakov, G. Grosse, and M. N. Grigoriev (2013b), Short- and long-term thermo-erosion of ice-rich permafrost coasts in the Laptev Sea region, *Biogeosciences*, *10*, 4297–4318, doi:10.5194/bg-10-4297-2013.

Günther, F., P. P. Overduin, I. A. Yakshina, T. Opel, A. V. Baranskaya, and M. N. Grigoriev (2015), Observing Muostakh disappear: Permafrost thaw subsidence and erosion of a ground-ice-rich island in response to arctic summer warming and sea ice reduction, *Cryosphere*, *9*, 151–178, doi:10.5194/tc-9-151-2015.

Harrison, W. D., and T. E. Osterkamp (1982), Measurements of the electrical conductivity of interstitial water in subsea permafrost, in *Proceedings 4th International Conference on Permafrost*, pp. 229–237, National Acad. Press, Wash.

Heim, B., et al. (2014), Ocean colour remote sensing in the southern Laptev Sea: Evaluation and applications, *Biogeosci. Discuss.*, *10*, 4191–4210, doi:10.5194/bg-11-4191-2014.

Hodgkins, S. B., M. M. Tfaily, C. K. McCalley, T. A. Logan, P. M. Crill, S. R. Saleska, V. I. Rich, and J. P. Chanton (2014), Changes in peat chemistry associated with permafrost thaw increase greenhouse gas production, *Proc. Natl. Acad. Sci. U.S.A.*, *111*(16), 5819–5824, doi:10.1073/pnas.1314641111.

Hutter, K., and B. Straughan (1999), Models for convection in thawing porous media in support for the subsea permafrost equations, *J. Geophys. Res.*, *104*(B12), 29,249–29,260, doi:10.1029/1999JB900288.

Jørgensen, B. B. (1982), Mineralization of organic matter in the sea bed—The role of sulphate reduction, *Nature*, *296*, 643–645.

Judd, A. G. (2004), Natural seabed gas seeps as sources of atmospheric methane, *Environ. Geol.*, *46*, 988–996, doi:10.1007/s00254-004-1083-3.

Katasonov, E. M., and G. G. Pudov (1972), Kriolitologicheskie issledovaniya v raione Van'kinoi guby morya Laptevykh (Cryolithological research in the Van'kina Guba area, Laptev Sea), Merzlotnye Issledovaniya (Permafrost Research) XII [in Russian], 130–136, Moscow State Univ.

Knittel, K., and A. Boetius (2009), Anaerobic oxidation of methane: Progress with an unknown process, *Annu. Rev. Microbiol.*, *63*, 311–334, doi:10.1146/annurev.micro.61.080706.093130.

Knoblauch, C., C. Beer, A. Sosnin, D. Wagner, and E.-M. Pfeiffer (2013), Predicting long-term carbon mineralization and trace gas production from thawing permafrost of northeast Siberia, *Global Change Biol.*, *19*(4), 1160–1172, doi:10.1111/gcb.12116.

Koch, K., C. Knoblauch, and D. Wagner (2009), Methanogenic community composition and anaerobic carbon turnover in submarine permafrost sediments of the Siberian Laptev Sea, *Environ. Microbiol.*, *11*(3), 657–668, doi:10.1111/j.1462-2920.2008.01836.x.

Konishchev, V. N., and S. F. Kolesnikov (1981), Osobennosti stroeniya i sostava pozdnekainozoiskikh otlozheniyakh v obnazhenii Oyogosskii Yar (Specifics of structure and composition of late Cenozoic deposits in the section of Oyogossky Yar), Problemy kriolitologii (Problems of Cryolithology), IX [in Russian], 107–117.

Kunitsky, V. V. (1989), *Kriolitologiya nizov'ya leny (Crylolithology of the Lower Lena)* [in Russian], 162 pp., SB RAS Mel'nikov Permafrost Institute Yakutsk, Russia.

Lantuit, H., et al. (2012), The Arctic coastal dynamics database: A new classification scheme and statistics on Arctic permafrost coastlines, *Estuaries Coasts*, *35*(2), 383–400, doi:10.1007/s12237-010-9362-6.

Lovley, D. R., D. F. Dwyer, and M. J. Klug (1982), Kinetic analysis of competition between sulfate reducers and methanogens for hydrogen in sediments, *Appl. Environ. Microbiol.*, *43*(6), 1373–1379.

McGuire, A. D., L. G. Anderson, T. R. Christensen, S. Dallimore, L. Guo, D. J. Hayes, M. Heimann, T. D. Lorenson, R. W. Macdonald, and N. Roulet (2009), Sensitivity of the carbon cycle in the Arctic to climate change, *Ecol. Monogr.*, *79*, 523–555, doi:10.1890/08-2025.1.

Meister, P., B. Liu, T. G. Ferdelman, B. B. Jørgensen, and A. Khalili (2013), Control of sulphate and methane distributions in marine sediments by organic matter reactivity, *Geochim. Cosmochim. Acta*, *104*, 183–193, doi:10.1016/j.gca.2012.11.011.

Meyer, H., L. Schönicke, U. Wand, H.-W. Hubberten, and H. Friedrichsen (2000), Isotope studies of hydrogen and oxygen in ground ice experiences with equilibration technique, *Isot. Environ. Health Stud.*, *36*, 133–149, doi:10.1080/10256010008032939.

Morgenstern, A., M. Ulrich, F. Günther, S. Roessler, I. V. Federova, N. A. Rudaya, S. Wetterich, J. Boike, and L. Schirrmeister (2013), Evolution of thermokarst in East Siberian ice-rich permafrost: A case study, *Geomorphology*, *201*, 363–379, doi:10.1016/j.geomorph.2013.07.011.

Nicolsky, D. J., V. E. Romanovsky, N. N. Romanovskii, A. L. Kholodov, N. E. Shakhova, and I. P. Semiletov (2012), Modeling sub-sea permafrost in the East Siberian Arctic shelf: The Laptev Sea region, *J. Geophys. Res.*, *117*, F03028, doi:10.1029/2012JF002358.

Niessen, F., et al. (2013), Repeated Pleistocene glaciation of the East Siberian continental margin, *Nat. Geosci.*, *6*(10), 842–846, doi:10.1038/ngeo1904.

O'Connor, F. M., et al. (2010), Possible role of wetlands, permafrost, and methane hydrates in the methane cycle under future climate change: A review, *Rev. Geophys.*, *48*, RG4005, doi:10.1029/2010RG000326.

Osterkamp, T. E. (2001), Sub-sea permafrost, in *Encyclopedia of Ocean Sciences*, vol. 5, edited by J. H. Steele, S. A. Thorpe, and K. K. Turekian, pp. 2902–2912, Acad. Press, New York, and London.

Overduin, P. P., H.-W. Hubberten, V. Rachold, N. N. Romanovskii, M. N. Grigoriev, and M. Kasymskaya (2007), The evolution and degradation of coastal and offshore permafrost in the Laptev and East Siberian Seas during the last climatic cycle, in *Coastline Changes: Interrelation of Climate and Geological Processes*, *Geol. Soc. Am. Spec. Pap.*, edited by J. Harff, W. W. Hay, and D. M. Tetzlaff, vol. 426, pp. 97–111, doi:10.1130/2007.2426(07).

Overduin, P. P., S. Westermann, K. Yoshikawa, T. Haberlau, V. Romanovsky, and S. Wetterich (2012), Geoelectric observations of the degradation of nearshore submarine permafrost at Barrow (Alaskan Beaufort Sea), *J. Geophys. Res.*, *117*, F02004, doi:10.1029/2011JF002088.

Popp, T. J., J. P. Chanton, G. J. Whiting, and N. Grant (1999), Methane stable isotope distribution at a Carex dominated fen in north central Alberta, *Global Biogeochem. Cycles*, *13*(4), 1063–1077, doi:10.1029/1999GB900060.

Preuss, I., C. Knoblauch, J. Gebert, and E.-M. Pfeiffer (2013), Improved quantification of microbial CH_4 oxidation efficiency in arctic wetland soils using carbon isotope fractionation, *Biogeosciences*, *10*(4), 2539–2552, doi:10.5194/bg-10-2539-2013.

Romanovskii, N. N., and H.-W. Hubberten (2001), Results of permafrost modelling of the lowlands and shelf of the Laptev Sea region, Russia, *Permafrost Periglacial Processes*, *12*, 191–202, doi:10.1002/ppp.387.

Romanovskii, N. N., H.-W. Hubberten, A. V. Gavrilov, V. E. Tumskoy, and A. L. Kholodov (2004), Permafrost of the East Siberian Arctic shelf and coastal lowlands, *Quat. Sci. Rev.*, *23*, 1359–1369, doi:10.1016/j.quascirev.2003.12.014.

Ruppel, C. (2014), Permafrost-associated gas hydrate: Is it really approximately 1% of the global system?, *J. Chem. Eng. Data*, *60*, 429–436, doi:10.1021/je500770m.

Ruppel, C. D. (2011), Methane hydrates and contemporary climate change, *Nat. Ed. Knowledge*, *3*(10), 29.

Schirrmeister, L., et al. (2003), Late Quaternary history of the accumulation plain north of the Chekanovsky Ridge (Lena Delta, Russia): A multidisciplinary approach, *Polar Geogr.*, *27*, 277–319.

Schirrmeister, L., et al. (2008), Periglacial landscape evolution and environmental changes of Arctic lowland areas for the last 60 000 years (western Laptev Sea coast, Cape Mamontov Klyk), *Polar Res.*, *27*, 249–272, doi:10.1111/j.1751-8369.2008.00067.x.

Schirrmeister, L., V. V. Kunitsky, G. Grosse, S. Wetterich, H. Meyer, G. Schwamborn, O. Babyi, A. Derevyagin, and C. Siegert (2011a), Sedimentary characteristics and origin of the late Pleistocene Ice Complex on northeast Siberian Arctic coastal lowlands and islands—A review, *Quat. Int.*, *241*, 3–25, doi:10.1016/j.quaint.2010.04.004.

Schirrmeister, L., G. Grosse, S. Wetterich, P. P. Overduin, J. Strauss, E. A. G. Schuur, and H.-W. Hubberten (2011b), Fossil organic matter characteristics in permafrost sequences of the northeast Siberian Arctic, *J. Geophys. Res.*, *116*, G00M02, doi:10.1029/2011JG001647.

Schirrmeister, L., et al. (2011c), Late Quaternary paleoenvironmental records from the western Lena Delta, Arctic Siberia, *Palaeogeogr. Palaeoclimatol. Palaeoecol.*, *299*, 175–196, doi:10.1016/j.palaeo.2010.10.045.

Shakhova, N., I. Semiletov, A. Salyuk, V. Yusupov, D. Kosmach, and Ö. Gustafsson (2010), Extensive methane venting to the atmosphere from the sediments of the East Siberian Arctic shelf, *Science*, *327*(5970), 1246–1250, doi:10.1126/science.1182221.

Shakhova, N., et al. (2014), Ebullition and storm-induced methane release from the East Siberian Arctic shelf, *Nat. Geosci.*, *7*(1), 64–70, doi:10.1038/ngeo2007.

Slagoda, E. A. (2004), *Kriolitogennye otlozheniya promorskoi ravnony morya laptevykh: litologia i mikromorfologiya (Cryolithogenic Deposits of the Laptev Sea Coastal Plain: Lithology and Micromorphology)* [in Russian], 119 pp., Ekspress, Tyumen, Russia.

Strauss, J., L. Schirrmeister, G. Grosse, S. Wetterich, M. Ulrich, U. Herzschuh, and H.-W. Hubberten (2013), The deep permafrost carbon pool of the Yedoma region in Siberia and Alaska, *Geophys. Res. Lett.*, *40*, 6165–6170, doi:10.1002/2013GL058088.

Taylor, A. E., S. R. Dallimore, R. D. Hyndman, and F. Wright (2004), Comparing the sensitivity of permafrost and marine gas hydrate to climate warming, in *Scientific Results From the Mallik 2002 Gas Hydrate Production Research Well Program, Mackenzie Delta, Northwest Territories, Canada*, *Geol. Surv. Can. Bull.*, vol. 585, edited by S. R. Dallimore and T. S. Collett, pp. 1–11.

Tumskoy, V. E. (2012), Osobennosti kriolitogeneza otlozhenii severnoi Yakutii v srednem Neopleistotsene-Golotsene (Peculiarities of cryolithogenesis in northern Yakutia from the Middle Neopleistocene to the Holocene) [in Russian], *Earth's Cryosphere*, *16*, 12–21.

Wetterich, S., S. Kuzmina, A. A. Andreev, F. Kienast, H. Meyer, L. Schirrmeister, T. Kuznetsova, and M. Sierralta (2008), Palaeoenvironmental dynamics inferred from late Quaternary permafrost deposits on Kurungnakh Island (Lena Delta, northeast Siberia, Russia), *Quat. Sci. Rev.*, *27*, 1523–1540, doi:10.1016/j.quascirev.2008.04.007.

Wetterich, S., P. P. Overduin, and M. N. Grigoriev (Eds.) (2011), Russian-German Cooperation System Laptev Sea: The Expedition eastern Laptev Sea - Buor Khaya Peninsula 2010, Berichte zur Polar- und Meeresforschung, 629.

Whalen, S. C., and W. S. Reeburgh (2000), Methane oxidation, production, and emission at contrasting sites in a boreal bog, *Geomicrobiol. J.*, *17*(3), 237–251.

Whiticar, M. J. (1999), Carbon and hydrogen isotope systematics of bacterial formation and oxidation of methane, *Chem. Geol.*, *161*(1–3), 291–314, doi:10.1016/S0009-2541(99)00092-3.

Winterfeld, M., L. Schirrmeister, M. N. Grigoriev, V. V. Kunitsky, A. A. Andreev, A. Murray, and P. P. Overduin (2011), Coastal permafrost landscape development since the late Pleistocene in the western Laptev Sea, Siberia, *Boreas*, *40*, 697–713, doi:10.1111/j.1502-3885.2011.00203.x.

Yakushev, V. S., and E. M. Chuvilin (2000), Natural gas and gas hydrate accumulations within permafrost in Russia, *Cold Reg. Sci. Technol.*, *31*, 189–197, doi:10.1016/S0165-232X(00)00012-4.

Yamamoto, S., J. B. Alcauskas, and T. E. Crozier (1976), Solubility of methane in distilled water and seawater, *J. Chem. Eng. Data*, *21*(1), 78–80, doi:10.1021/je60068a029.

Zhigarev, L. A. (1997), *Submarine Cryolithozone (Okeanicheskaya kriolitozona)* [in Russian], 320 pp., Moscow State Univ. Publ., Moscow.

Zhigarev, L. A. (1998), Osobenosti dinamiki beregovoi kriolitozony arkticheskikh morei (Characteristics of the coastal dynamics in the permafrost zone of arctic seas), in *Dynamics of the Arctic Coasts of Russia* [in Russian], pp. 19–34, Moscow State Univ. Publ., Moscow.